



# Seismic Response Investigation and Nonlinear Numerical Analysis of Cold-Formed Thin-Walled Steel Tube Truss Shear Walls

Jingfeng Wang<sup>1,2</sup> · Wanqian Wang<sup>1</sup> · Shuai Pang<sup>1</sup> · Bo Yu<sup>1</sup>

Received: 12 June 2018 / Accepted: 10 April 2019 / Published online: 22 April 2019  
© Korean Society of Steel Construction 2019

## Abstract

In order to satisfy the requirements of seismic capacity of cold-formed thin-walled steel structure in low- and multi-rise buildings, an innovative cold-formed thin-walled steel tube truss (CFSTT) shear wall sheathed with both-side oriented strand board (OSB) was proposed in this paper. Five full-scale specimens of CFSTT shear walls which composed of square cold-formed thin-walled steel tubes, tracks, galvanized V-shaped connectors and OSB panels were tested under low-cyclic loading. The seismic performance of CFSTT shear wall was evaluated in terms of hysteretic behavior, envelop curves, ductility and energy dissipation, etc. Then, a practical nonlinear simplified analysis method of CFSTT shear walls under low-cyclic reversed lateral loading was proposed based on the principle of equivalent tie rod model. The double- and four-limb lattice studs were also simplified as single steel tubes. Besides, a pivot modeling approach was suggested to stimulate the sheathing-to-frame connection. Subsequently, the finite element models of CFSTT shear walls were established based on this simplified method and verified by the experimental data. Numerical and experimental results indicated that CFSTT shear walls exhibited excellent seismic performance, and the accuracy of the simplified of lattice stud was verified. Furthermore, the simplified method proposed in this paper will highly facilitate conducting the nonlinear analysis for shear walls.

**Keywords** Cold-formed thin-walled steel tube truss (CFSTT) shear walls · Seismic performance · Simplified model · Pivot model · Numerical analysis

## 1 Introduction

In recent years, greater attention has been paid to the innovation of prefabricated structures in China and other countries owing to the development of building industrialization. The cold-formed thin-walled steel (CFS) structure was popularly adopted in the low-rise and multi-rise buildings accounting for its prior structural superiorities, such as environmental friend, lightweight, easy installation, and low cost. Traditionally, the cold-formed steel C-section (C-steel) was popularly used as a main load bearing component. However, it is well known that the C-steel exhibits poor torsional performance under bending and compressive loads. Thus, employing C-steel as wall stud of cold-formed thin-walled

steel structures may be liable to fail under low cyclic loads, and this type of structure need to be strengthened to improve the torsional resistance and seismic behaviors.

One effective method, which originated from Canada (CAN/CSA S136-01), to cover the shortcoming of the cold-formed thin-walled structures employing C-steel is using square steel tube as its wall studs instead of C-steel. Cold-formed thin-walled steel tube truss (CFSTT) structure behaves all advantages of conventional CFS structure and moreover shows better architectural aesthetics appearance, good economical efficiency, superior structural stability as well as convenient for setting interior pipeline. Moreover, the CFSTT shear wall is the main lateral load bearing structural component in the CFSTT structure. It developed from the traditional CFS shear walls mainly consist of double-side oriented strand board (OSB), double- or four-limb lattice studs, top and bottom tracks (as seen in Fig. 1). Besides, the interior wall studs are composed of double square tubes and galvanized V-shaped connectors, and the studs in the wall end and opening edge are composed of four square tubes and galvanized V-shaped connectors. The OSB panels were

✉ Jingfeng Wang  
jfwang008@163.com

<sup>1</sup> School of Civil Engineering, Hefei University of Technology, Hefei 230009, Anhui Province, China

<sup>2</sup> Anhui Civil Engineering Structures and Materials Laboratory, Hefei 230009, Anhui Province, China

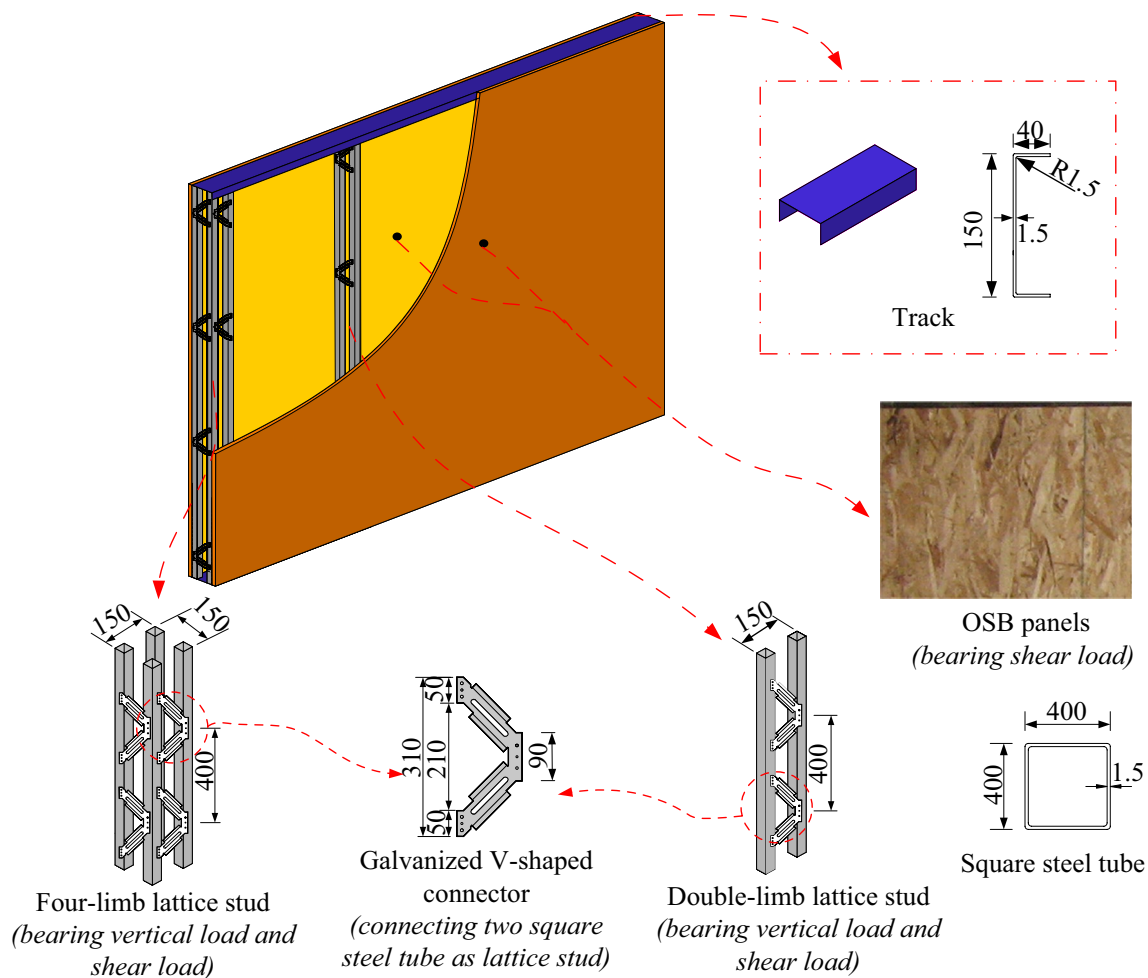


**Fig. 1** Main members of CFSTT shear wall

attached to the CFSTT frame by self-drilling screws. As an industrial and natural green building, the CFSTT structure was extensively used in Canada (CAN/CSA S136-01), American (AISI-S213-07/S1-09), and China (DB34/T1262-2010; Wang et al. 2019).

Up till now, many researchers concerned on the details of CFS beams, such as Li et al. (2016), Obst et al. (2016), Magnucka-Blandzi and Magnucki (2011) and Ostwald and Rodak (2013). A series of studies have been conducted to analyze CFS columns, such as Li et al. (2014) and Shahbazian and Wang (2012). Apart from these studies, many investigations had been carried out on CFS shear walls, and most of the studies focused on the CFS shear walls. The static performance of the CFS shear walls were respectively explored by Langea and Naujoks (2006), Lee and Miller (2001) and Tian et al. (2007). Besides, a plenty of studies on the hysteretic response of the CFS shear walls, such as Wang et al. (2016), Nithyadharan and Kalyanaraman (2012) and Mohebbi et al. (2015), had been researched. Moreover, the shake table tests were also conducted on cold-formed

steel framed buildings by Schafer et al. (2016) and Kim et al. (2006). Apart from above-mentioned work, extensive investigations have been carried out on kinds of alternatives to the CFS shear walls. Casafont et al. (2006) studied the performance of screwed connectors and Fiorino et al. (2016) researched the influence of strap-braced on the global response.

Compared to the large amount of literature on CFS members, shear walls and structures presently, the researches on CFSTT shear walls was scarce. Considering the cyclic loading tests on full-scale specimens with the shortages of high cost and long experimental period, the method of numerical modeling could be adopted to predict the shear response of CFS shear wall accurately (Buonopane et al. 2015; Peterman et al. 2014; Zeynalian and Ronagh 2012; Fiorino et al. 2018). As shown in Niari et al. (2015), the numerical results were coincide with test data, so the finite element (FE) models could be used to stimulate the seismic response of CFS shear walls sheathed with steel panel. Three different numerical FE models are presented in Fülöp and

Dubina (2004), which distinct with each other in terms of complexity and the ability to simulate nonlinear monotonic or cyclic lateral response. Consequently, determining the shear response of this type of wall and developing its FE model is an exceedingly effective and reliable method for in-depth studies to better understanding the structure behavior of CFS shear walls in seismic analysis. However, due to the inherent complex of CFSTT shear wall, the detailed FE model is time-consuming and the stimulated results are not prone to convergence. Therefore, in an attempt to explore the seismic response of CFSTT shear walls efficiently, the necessity of developing a simplified analysis modeling was emerged.

The main object of this paper was to make a further investigation on the seismic response of CFSTT shear walls. Hereinto, five full-scale CFSTT shear wall specimens with double-side OSB sheathings were tested under vertical axial compression combining lateral cyclic load. Moreover, a simplified analytical method was proposed to efficiently explore the seismic response of CFSTT shear wall and to come up with the interaction between the complex components. FE modeling on the base of the simplified model and pivot model was developed to stimulate the seismic behavior of CFSTT shear wall, and the numerical analytical and test results had been compared. The results demonstrated that the nonlinear simplified model could well predict the seismic performance of the CFSTT shear walls. Of particular interest was the simplified method of CFSTT shear walls and this paper give suitable indications for practical applications.

## 2 Experimental Programs

### 2.1 Test Specimens

According to practical engineering, five single-storey full-scale CFSTT shear walls sheathed with double-side OSB panels were tested and analyzed in this section to explore seismic performance of the type of shear walls. Five shear wall specimens with identification numbers CFSTT1, CFSTT2, CFSTT3, CFSTT4 and CFSTT5 were tested according to specification JGJ/T 101-2015. Five specimens were tested with different assemblies under axial compression combining lateral low-cyclic load to stimulate seismic loading conditions in Anhui Civil Engineering Structures and Materials Laboratory. All specimens were assembled with a rectangular geometry 4200 mm wide and 3250 mm high. The height-width ratio of shear wall is determined according to the engineering practice, and the commonly used height-width ratio ranges from 0.5 to 1.5. The size of 4200 mm wide and 3250 mm high was selected within the commonly scope. The connection with the bottom beam were determined according to some practical engineering.

The thickness of all specimens was 150 mm. Double-side OSB panels were used in this test as sheathing according to present engineering and also owing to its high bearing capability. In order to provide experimental and analytical data for engineers, it is notably essential to develop researches with respect to CFSTT shear walls with openings. In terms of the specimens with openings, the opening rate was defined as the ratio of the total opening area to the area of CFSTT shear wall. Specimens CFSTT2-CFSTT5 had different type of wall openings with the opening rate of 13.8%, 13.9%, 27.8% and 54.6%, respectively. The configuration details of test specimens were illustrated in Fig. 2, and detail specimen information, including the opening size, opening area ratio and sheathing type were listed in Table 1.

The studs of the shear walls were mainly composed of two or four square cold-formed thin-walled steel tubes  $40 \times 40 \times 1.5$  mm (width  $\times$  height  $\times$  thickness), which were connected by galvanized V-shaped connectors (1.5 mm). The interior wall studs were double-limb lattice studs, while the end wall studs and opening edge studs were four-limb lattice studs. X-shaped bracing were set up between OSB panels and CFS framing. Additionally, the thickness in all OSB panel is 8 mm and the cross section of X-shaped bracing is  $100 \times 1.5$  mm. The ST4.2 self-drilling screws connected the OSB panels to the CFSTT frame spaced at 150 mm along the perimeter and spaced at 300 mm at the middle of wall. The connections of steel strips and framing were strengthened by steel gusset plate. The bottom track of specimens was fastened to foundation beam by anchor bolts.

### 2.2 Material Properties

The coupons tests of steel material properties of the CFSTT components were carried out according to the specification GB/T228.1-2010. The yield stress ( $f_y$ ), the ultimate stress ( $f_u$ ), Young's modulus ( $E$ ), and the elongation at fracture ( $\delta$ ) of steel components, including steel trips, square steel tubes, galvanized V-shaped connector and channels, were obtained from material tests. The material property results which employed in the specimens have been summarized in Table 2.

The yield strength and the elastic modulus of the OSB panel were determined by a three-point bending system of universal material testing machine according to the specification GB/T 17657. The yield strength and elastic modulus of OSB panel were respectively  $22 \text{ N/mm}^2$  and  $3500 \text{ N/mm}^2$ ; the Poisson's ratio was 0.3. The material properties of OSB panel meet the requirement of LY/T 1580-2010. The elastic modulus represented the equivalent Young's modulus of the OSB panels.

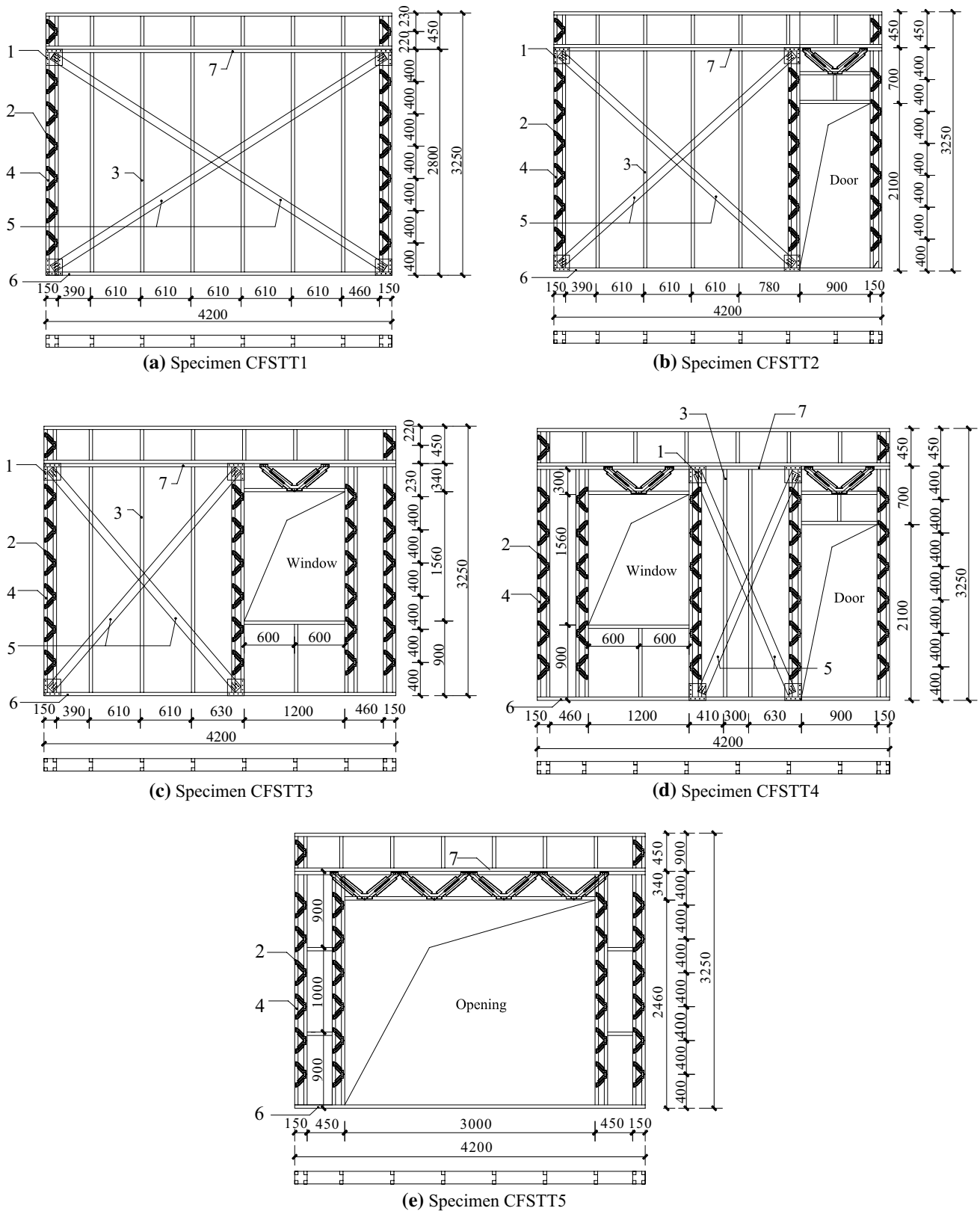


**Fig. 2** Details of wall specimens (units: mm). *Note* 1—gusset plate, 2—galvanized V-shaped connector, 3—double-limb latticed stud, 4—four-limb latticedstud, 5—X-shaped bracing, 6—bottom track, 7—top track

**Table 1** Information of the test specimens

Specimen label	Opening size (mm × mm)		Opening area ratio	Panel type	Sheathing type
	Door	Window			
CFSTT1	–	–	–	OSB	Double side
CFSTT2	900 × 2100	–	13.8%	OSB	Double side
CFSTT3	–	1200 × 1560	13.9%	OSB	Double side
CFSTT4	900 × 2100	1200 × 1560	27.8%	OSB	Double side
CFSTT5	3000 × 2420	–	54.6%	OSB	Double side

**Table 2** Material properties of steel

Steel components	Thickness <i>t</i> /mm	Yield strength $f_y$ /(N/mm <sup>2</sup> )	Tensile strength $f_u$ /(N/mm <sup>2</sup> )	Young's modulus $E$ /(N/mm <sup>2</sup> )	Elongation at fracture $\delta$ (%)
Steel trip	1.5	216	314	$1.85 \times 10^5$	32
Square steel tubular	1.5	300	330	$2.02 \times 10^5$	19
Galvanized V-shaped Connectors	1.5	361	374	$2.45 \times 10^5$	19
Track	1.5	305	333	$2.03 \times 10^5$	20

### 2.3 Test Setup and Loading Protocol

The photo and general diagram of the test setup are shown in Fig. 3. A 500 kN hydraulic jack was suspended off the reaction beam and was placed on the top spreader beam to apply vertical loads. Besides, vertical loads were transmitted to the specimens via distributive girder. The axial pressure of 170 kN together with the weight of distributive girder was an average force in consideration of the live and dead loads of the superstructure which stems from a two-story engineering practice. Horizontal cyclic displacements were imposed by a 1000 kN MTS hydraulic which mounted on the reaction wall with a  $\pm 250$  mm displacement range. All tests loading were controlled by displacement. Four 32 mm diameter steel bars was used to transfer load between hydraulic actuator and specimen. The bottom foundation beam was used to simulate a rigid foundation and fix the shear wall on the floor; the displacement in three direction of the shear wall bottom was restricted by the tension anchors and bottom foundation beam (Fig. 3).

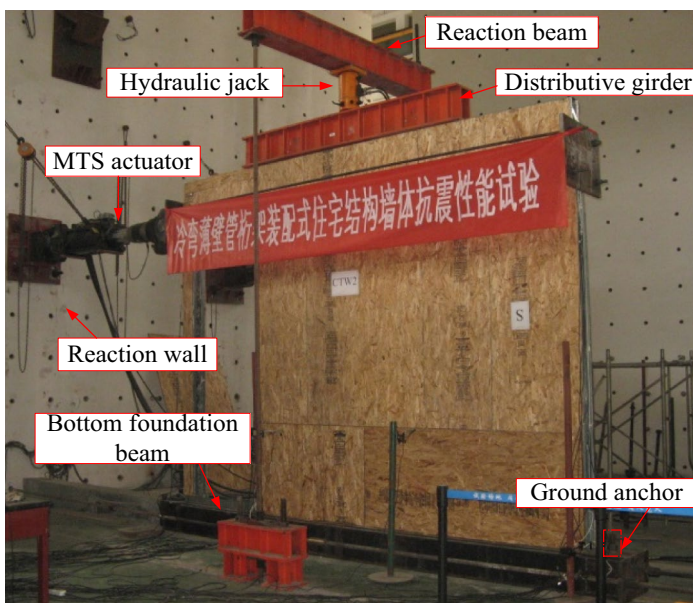
The loading history of the specimens was generally applied based on the specification ATC-24 (1992), which stipulated the guidelines on cyclic loading of structural steel components. The loading history adopted in this experiment was shown in Fig. 4.  $\Delta_y$  was defined as the predicted yielding displacement corresponding to the predicted yielding load ( $P_y$ ), and  $P_y$  was approximately  $0.7P_{\max}$  ( $P_{\max}$  denotes the predicted shear bearing capacity on the basis of finite element analysis).

## 3 Analysis of Test Result

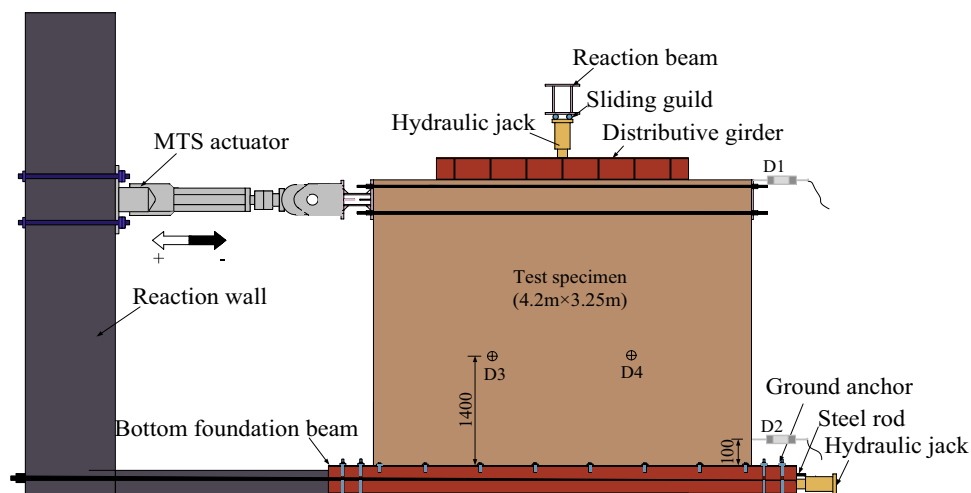
### 3.1 Load–Displacement Hysteretic Behavior

The force–displacement hysteresis relationship can reflect the cyclic performance of the CFSTT shear walls obviously. The load versus displacement ( $P$ – $\Delta$ ) hysteretic curves for each individual test specimen under cyclic loads can be shown in Fig. 5. The key points a to e marked in the curves illustrated failure modes and processes of the specimens. At low load levels, the hysteresis curve showed shuttle-shape, and the residual deformation was observed when unloading to zero force. Then, an increase in the amount of OSB panel cracks resulted in a turning point in the curves, which demonstrated that the specimens entered the yield stage. After the yield stage, the hysteresis curves showed nonlinearity after a short-term elastic range due to the tilt and further pull-out of the screws. As the failure of screw connections and the relative slips between sheathings observed, the hysteretic curve showed a phenomenon of significant pinching, which is caused by opening and closing of the screw holes. The shapes of the curves were stable and plentiful with a noticeable pinching effect, so the curves transformed from linear to spindle-shaped. Beyond the peak load, the curves exhibited strength degradation and it mainly attributed to relative slippage between the OSB panels and framing. When the later loading reached to the peak point, the strength and the area of the hysteretic loop decreased gradually in successive cycles owing to the sheathing demolition and

Fig. 3 Experimental setup



(a) Overview of test specimen



(b) Diagram of experimental setup

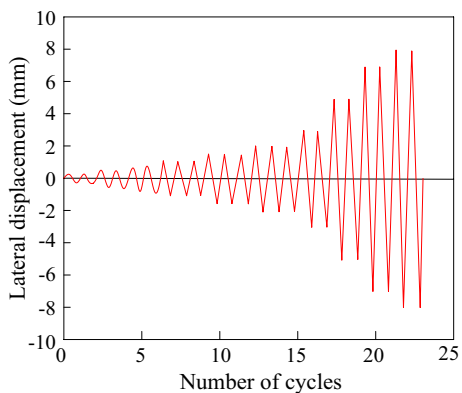
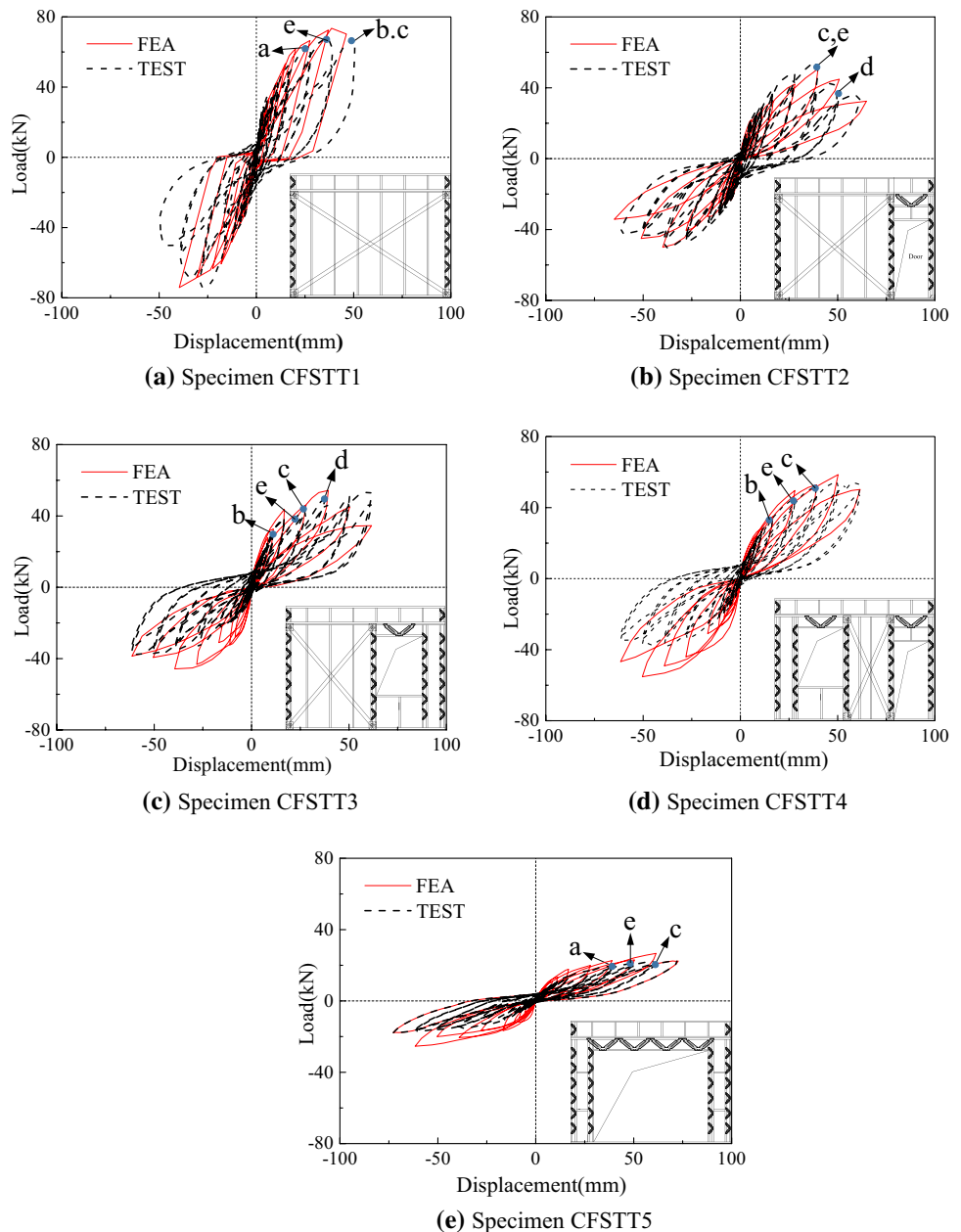


Fig. 4 Loading history

pulled out of screws through the OSB panels, which demonstrated the strength degradation of the specimen. In general, specimen CFSTT1 have a plumper hysteretic loops compared with other specimens, which indicates the wall with the smaller opening area has a more excellent energy dissipation capacity. The above finding shows that opening would reduce the bearing capacity and lateral stiffness of the wall. Moreover, it is evident from the comparison of CFSTT1 and CFSTT5 that the large opening has more obvious detrimental influence on the elastic stiffness and shear bearing capacity of CFSTT shear wall. It is recommended that the suitable measures are needed to be taken to improve the seismic behavior of CFSTT shear wall with openings.

**Fig. 5** Predicted and tested later load versus displacement hysteretic curves. *Note* a—cracking of OSB panel, b—yielding of steel strip, c—screw pull-through and detachment of panel from frame, d—rupturing of steel strip, e—buckling of track



### 3.2 Load–Displacement Envelope Curves

The horizontal load versus displacement envelope curves (illustrated in Fig. 6) of all specimens were created by connecting each peak load point at each displacement level based on the load versus displacement hysteretic curves in Fig. 5. During the low load levels, all specimens showed an approximate linear relationship before the lateral displacement reaches the peak point. With the load increasing, specimen entered the elastic–plastic stage and the load showed a nonlinear relationship with the displacement due to cracks of the OSB panels and pulled out of screws. Three typical characteristic points were obtained based on the specification

JGJ/T 101-2015 (as illustrated in Fig. 7) from the envelope curves to assess seismic behavior of the specimens quantitatively, and the results were summarized in Table 3. The characteristic values of loads and displacements include yield load  $P_{y,t}$ , peak load  $P_{m,t}$  and failure load  $P_{f,t}$ , as well as the corresponding net lateral displacements  $\Delta_y$ ,  $\Delta_{m,t}$  and  $\Delta_{f,t}$ . Specimen CFSTT1 showed greatest shear bearing capacity and elastic stiffness among all specimens, while specimens CFSTT5 exhibited the least shear bearing capacity and elastic stiffness owing to largest opening ratio. It indicated that the wall opening decreased the bearing capacity as well as elastic stiffness. Therefore, the large opening had more obvious detrimental influence on the seismic behavior of CFSTT

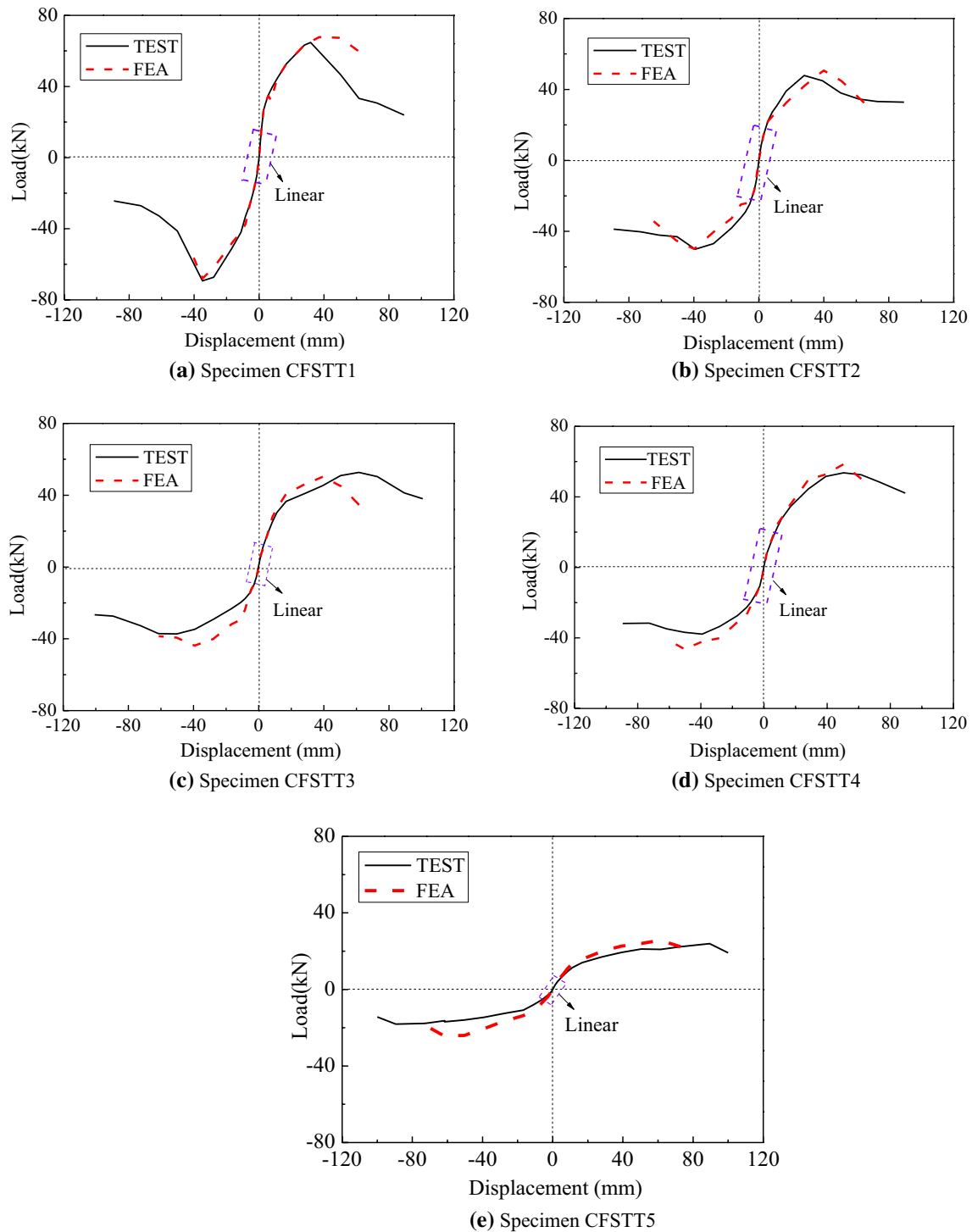


Fig. 6 Predicted and tested later load versus displacement envelope curves

shear wall. It was recommended the suitable measurement, such as setting four-limb latticed studs at the boundaries of the opening, needed to be taken to enhance the seismic behavior of CFSTT shear wall with openings and avoid early local buckling of the studs.

### 3.3 Ductility

The displacement ductility factor ( $\mu$ ), namely  $\mu = \Delta_{u,t} / \Delta_{y,t}$ , was employed to evaluate the ductility property of this type of shear wall. Up till now, there is short of the detailed ductility



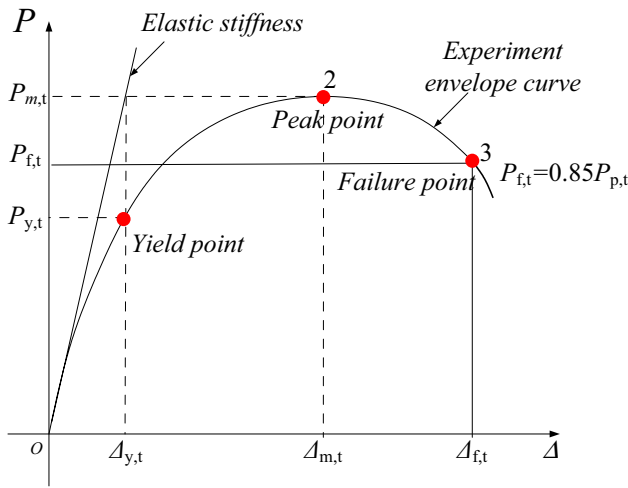


Fig. 7 Characteristic points of specimens

index for the CFS structures. The ductility factors  $\mu$  of the composite walls were listed in Table 4. The test results exhibited that the ductility factor ( $\mu$ ) of five specimens was within the confines of 4.28–9.03. Cyclic tests of CFCS shear walls with four different types of sheathing were conducted by Ye et al. (2016). The ductility factor of specimens in Ye et al. (2016) was within the scope of 1.49–4.11. The comparison between the results of this paper and Ye et al. (2016) indicated that the CFSTT shear wall exhibited greater ductility and could meet ductility design requirements for seismic design of structures at acceptable levels of displacement. Table 3 showed the ductility of specimens CFSTT2, CFSTT3, CFSTT4 and CFSTT5 are visibly raised, compared to specimen CFSTT1. The evidence indicated that wall opening and four-limb lattice stud had effect on the ductility of CFSTT shear wall. The specimens CFSTT2 and CFSTT3 had similar opening rate, while the ductility of specimen CFSTT3 with four four-limb latticed studs is enhanced, compared to specimen CFSTT2 with three four-limb latticed stud, which indicated adding the

Table 3 Characteristic values on envelop curves

Specimen	Yielding point		Peak point		Failure point		$\mu$
	$\Delta_{y,t}$ (mm)	$P_{y,t}$ (kN)	$\Delta_{m,t}$ (mm)	$P_{m,t}$ (kN)	$\Delta_{f,t}$ (mm)	$P_{f,t}$ (kN)	
CFSTT1 (+)	10	40.12	28	74.22	37	63.09	4.28
CFSTT1 (-)	8	33.04	28	74.10	41	62.99	4.88
CFSTT2 (+)	9	27.48	38	54.80	45	46.58	5.50
CFSTT2 (-)	8	29.16	38	50.56	56	42.98	6.64
CFSTT3 (+)	13	34.01	59	53.21	76	45.23	6.11
CFSTT3 (-)	8	17.62	59	37.76	76	32.10	9.03
CFSTT4 (+)	11	27.25	50	54.12	77	46.00	6.78
CFSTT4 (-)	9	20.16	38	38.15	72	32.43	8.15
CFSTT5 (+)	13	12.08	89	23.90	115	20.31	5.81
CFSTT5 (-)	11	8.11	90	18.07	97	15.36	8.71

Table 4 Energy dissipation parameters of specimens at ultimate state

Specimen	$\Delta/\Delta_y$	$W_{total}$ (kN mm)	$\xi_e$	$E_e$
CFSTT1 (+)	7	7204	0.28	1.74
CFSTT1 (-)	7	7204	0.28	1.74
CFSTT2 (+)	5	5136	0.29	1.81
CFSTT2 (-)	7	6950	0.27	1.69
CFSTT3 (+)	11	11078	0.22	1.37
CFSTT3 (-)	11	11,078	0.22	1.37
CFSTT4 (+)	11	8070	0.23	1.44
CFSTT4 (-)	9	6975	0.24	1.51
CFSTT5 (+)	16	9645	0.24	1.52
CFSTT5 (-)	16	9645	0.24	1.52

number of four-limb latticed studs can improve the ductility of the walls.

### 3.4 Energy Dissipation Capacity

Figure 8 showed the relationship between equivalent viscous damping factor ( $\xi_e$ ) and relative lateral displacement ( $\Delta/\Delta_y$ ) of all specimens. The equivalent viscous damping factor ( $\xi_e$ ), which was adopted in accordance with specification JGJ101 (1997), can be figured out by Eq. (1). Hereinto,  $S_{ABC}$  and  $S_{CDA}$  are respectively areas under curve ABC and CDA, as illustrated in Fig. 8 and  $S_{OBE}$  and  $S_{ODF}$  are respectively areas within triangles OBE and ODF.

$$\xi_e = \frac{1}{2\pi} \frac{S_{ABC} + S_{CDA}}{S_{OBE} + S_{ODF}} \tag{1}$$

The dissipated energy capability ( $E_e$ ) of each hysteretic loop was figured out by Eq. (2), and the results were described in Table 5.

$$E_e = 2\pi\xi_e \tag{2}$$

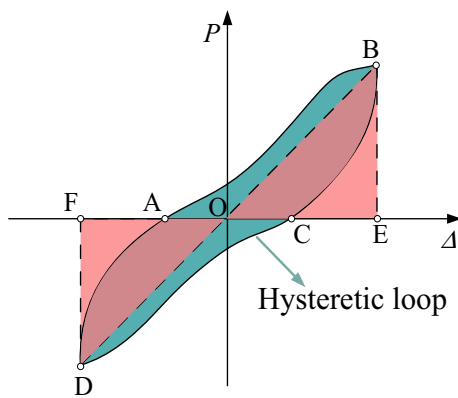


Fig. 8 Idealized  $P-\Delta$  hysteretic relationship

The cumulative dissipated energy  $W$  of tested specimens at each hysteretic loop was listed in Fig. 9. The total dissipation energy  $W_{total}$  is defined as the areas of the hysteresis curves when specimens at failure loading stage. Table 4 showed the total dissipation energy  $W_{total}$ , the equivalent viscous damping factor ( $\xi_e$ ) and the energy-dissipating capacity ( $E_e$ ) of specimens. As shown in Fig. 9 and Table 4, the total dissipation energy  $W_{total}$  of specimen CFSTT2 was lower than specimen CFSTT1. This indicated that the openings had negative impact to the energy dissipation capacity of CFSTT shear walls. Besides, the total dissipation energy  $W_{total}$  of specimens CFSTT3, CFSTT4 and CFSTT5 were higher than that of CFSTT2. It demonstrated that energy dissipation capacity can be improved by increasing the number of four-limb latticed stud. Moreover, the layout of opening should also be taken into consideration.

#### 4 Simplified Nonlinear Numerical Analysis of CFSTT Shear Walls

Due to the limitations of experimental studies in term of time and cost, it is useful to conduct numerical analysis for further studies revealing the response characteristics of the CFSTT shear walls. Flexible instruments requiring few parameters and allow computational effort, accompanied

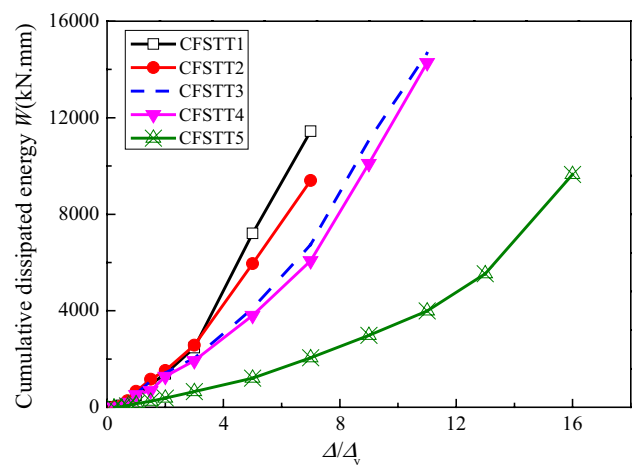


Fig. 9 Cumulative dissipated energy of test specimens

with sufficient reliability, appeared its necessity to perform nonlinear numerical analyses for CFSTT shear walls. At present, the numerical analysis CFSTT shear wall could be conducted via detailed FE model or equivalent bracing model. The detailed FE model can be developed in software ABAQUS and ANSYS, and the equivalent bracing model can be developed in software SAP2000. The detailed FE model were able to predict the seismic response and strain etc. of the shear wall, but the equivalent bracing model can obviously save workload and time. In this paper, an equivalent bracing model was adopted to simplify the shear wall in accordance with the deformation analysis. Besides, in order to simplify the CFSTT shear wall, a simplified method of latticed stud was put forward according to the section characteristics. Then, the Pivot model introduced by Meddah et al. (2016) based on the experimental results was employed to simulate the hysteretic relationships of the sheathing-to-frame connections. In attempt to determine the Pivot model for the CFSTT shear walls, the necessity of developing restoring force model on this type of shear was emerged. Details of the simplified approach were described in the following sub-sections.

Table 5 Equivalent later stiffness of shear wall

Type	$L$ (mm)	$H$ (mm)	$t$ (mm)	$G$ ( $N\ mm^{-2}$ )	$S_0$ (mm)	$n_N$	$f_N$ (N)	$EA_B$ (kN)	$K$ ( $N\ mm^{-1}$ )
CFSTT shear wall sheathed with single-side OSB panels	4200	3250	8	392	0.55	29	907	27,915,228	3288
CFSTT shear wall sheathed with double-side OSB panels	4200	3250	8 + 8	392	0.55	29	–	55,830,456	6576

### 4.1 Simplified Model of CFSTT Shear Wall

#### 4.1.1 Equivalent Bracing Model to the Shear Wall

The deformation of the shear wall under vertical axial compression combining lateral cyclic load mainly consists of three discrete components: actual shearing deformation, bending deformation and overturning deformation (as shown in Fig. 10). The equation of total deformation can be written as:

$$\Delta = \Delta_p + \Delta_N + \Delta_F + \Delta_R \tag{3}$$

where,  $\Delta$  is the measured deformation of shear wall;  $\Delta_p$  is actual shearing deformation of sheathing;  $\Delta_N$  is shearing deformation of self-drilling screw;  $\Delta_F$  and  $\Delta_R$  are bending deformation and overturning deformation of shear wall, respectively. The vertical deformation of shear wall was so small, so it was assumed to be zero in this paper.

The overturning deformation  $\Delta_R$  caused by the slipping of self-drilling screw is too small according to the experiments, so it can be neglected in the analysis. Besides, because of the high width to height ratio of specimens, the bending deformation  $\Delta_F$  is also so small that it was neglected. Therefore, the measured deformation of shear wall is mainly composed of  $\Delta_p$  and  $\Delta_N$ , that is  $\Delta = \Delta_p + \Delta_N$ . The present approach used

to analysis shear walls is equivalent bracing model. The principle of this method was considering the wall elements as a system of bar element, hinged with each other. According to the presented method, each shear wall element consisted of separate segments acting as tie rod. Figure 11 describes a simplified method of CFSTT shear wall. Particularly, the CFSTT shear wall was established as two-dimensional models with three degrees of freedom, including horizontal and vertical translation and in plane rotation. The axial deformations of the shear walls were so small when it was subjected to 170 kN according to practice and experiments. Moreover, according to Refs. Ye et al. (2015) and Xu et al. (2018), the influence of axial load is not considered when considering the shear deformation. Therefore, the axial deformation was not considered in this paper.

Assumptions for this method are as follows: (1) The sheathing is equivalent to a diagonal tie rod, which is assumed to be an important member to resist lateral load; (2) the tension and compression stiffness  $EA$  of the tie rod is calculated by the Eq. (7); (3) the members in the simplified model are connected with hinges owing to the self-drilling screws connection; (4) for members except for the tie rods, it is assumed that the tension and compression stiffness  $EA$  is far greater than that of the tie rods; (5) double- or

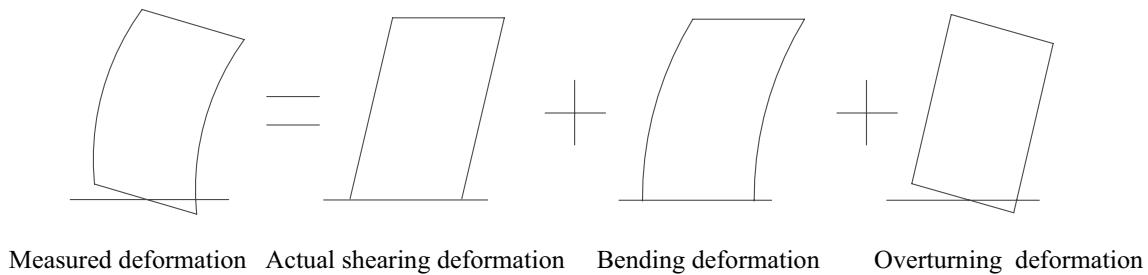
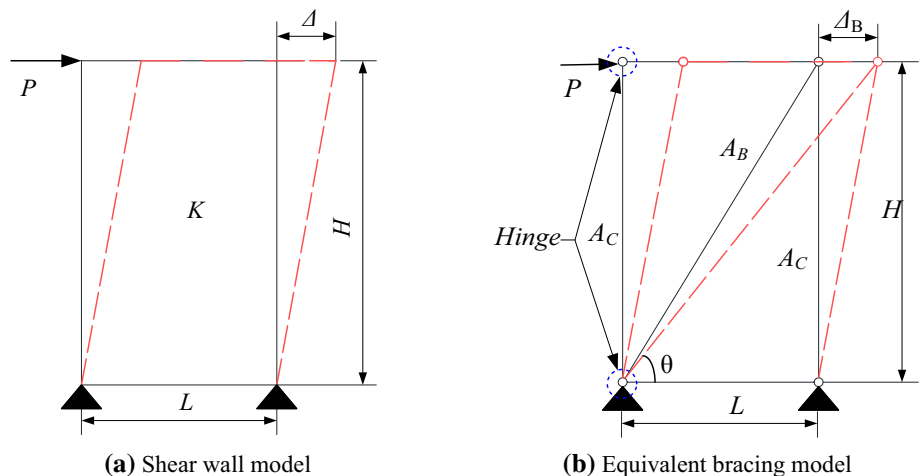


Fig. 10 Deformation of shear walls

Fig. 11 Basic principle of equivalent tie rod model



four-limb latticed stud can be simplified in accordance with the method described in Sect. 4.1.3.

### 4.1.2 Lateral Stiffness of Shear Wall

Ignoring the shearing deformation of self-drilling screw, the wall sheathing was equivalent to a diagonal tie rod by considering the actual shearing deformation of sheathing only. The shear walls and member systems have equivalent vertex horizontal displacement under the action of concentrated force  $P$  on the top (DB34/T1262-2010). Hence, on the base of geometrical and mechanical principle, the horizontal displacement of the simplified tie rod model under the same condition can be calculated in following form:

$$\Delta_B = \frac{(L^2 + H^2)^{1.5}}{L^2} \cdot \frac{P}{EA_B} \tag{4}$$

where,  $P$  is the top horizontal force of the shear wall;  $H$  is the height of shear wall;  $L$  is the length of shear wall;  $E$  is elastic modulus of tie rod;  $A_B$  is equal cross-section area. As mentioned above,  $\Delta = \Delta_B$  ( $\Delta_B$  is top lateral deformation of simplified model) in this paper and the tensile compression stiffness of tie rod can be written as:

$$EA_B = K \frac{(L^2 + H^2)^{1.5}}{L^2} \tag{5}$$

Then, taking the effect of sheathing type, sheathing thickness, screw slipping and screw spacing into consideration, the formula of  $EA_B$  can be further improved. The expression to obtain the actual shearing deformation of sheathing  $\Delta_p$  is summarized in (6).

$$\tau = G \cdot \gamma \tag{6-1}$$

$$\frac{P}{L \cdot t} = G \cdot \frac{\Delta_p}{H} \tag{6-2}$$

$$\Delta_p = \frac{PH}{LtG} \tag{6-3}$$

where,  $G$  is shear elastic modulus of wall sheathing;  $t$  is the thickness of sheathing.

In the shear wall element, the shearing deformation of self-drilling screw  $\Delta_N$  is calculated by the slipping of screws (Fig. 12). The ratio of  $L$  to  $H$  and the number of screws in length width direction is basically the same. It can be considered that each screw bears equal shearing force. When top horizontal force of the shear wall  $P$  is 1, the shear force on a single screw is  $\bar{q}_N = \frac{1}{n_N}$ . It is assumed that slipping of single screw under  $P$  is  $S_N$ . The shearing deformation of self-drilling

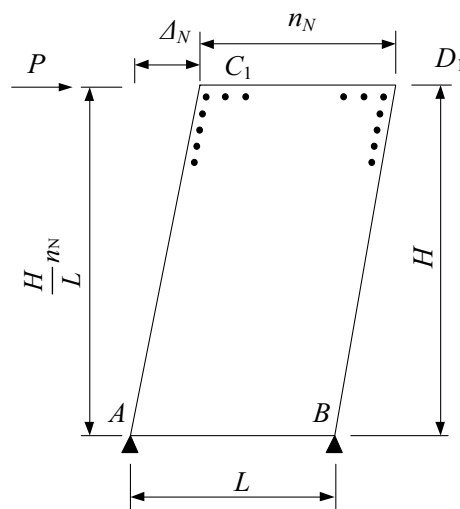


Fig. 12 Shearing deformation of self-drilling screw

screw  $\Delta_N$  is summarized in (7) based on the above assumptions and principle of virtual work.

$$1 \times \Delta_N = \sum S_N \bar{q}_N = 2n_N S_N \bar{q}_N + \frac{H}{L} S_N \bar{q}_N = 2S_N \left(1 + \frac{H}{L}\right) \tag{7-1}$$

$$\Delta_N = 2S_N \left(1 + \frac{H}{L}\right) \tag{7-2}$$

$$R_N = \frac{S_N}{S_\theta} = \frac{q_N}{f_N} \tag{7-3}$$

$$\Delta_N = 2S_\theta R_N \left(1 + \frac{H}{L}\right) = \frac{2S_\theta P}{n_N f_N} \left(1 + \frac{H}{L}\right) \tag{7-4}$$

$$\Delta_N = \frac{2S_\theta P}{n_N f_N} \left(1 + \frac{H}{L}\right) \tag{7-5}$$

where,  $f_N$  is shear bearing capacity of self-drilling screw;  $S_\theta$  is the overturning deformation of the self-drilling screw when it reaches to its shear capacity;  $n_N$  is the number of self-drilling screw towards the wide direction of the wall.

Hence, as for the model of shear wall which was under constant axial compression combining lateral low-cyclic load, the measured deformation of the vertex can be calculated adopting Eq. (8):

$$\Delta = \frac{P}{K} = \Delta_p + \Delta_N = \frac{PH}{LtG} + \frac{2S_\theta P}{n_N f_d} \left(1 + \frac{H}{L}\right) \tag{8}$$

Thus, according to the above three equation, lateral stiffness  $K$ , tensile compression stiffness  $EA_B$  can be expressed as Eq. (9) and (10). And the values of  $K$  and  $EA_B$  were calculated and listed in Table 5.

$$EA_B = \frac{(H^2 + L^2)^{1.5}}{\frac{HL}{Gt} + (HL + H^2) \frac{2S_\theta}{n_n f_N}} \tag{9}$$

$$K = \frac{L^2}{\frac{HL}{Gt} + (HL + H^2) \frac{2S_\theta}{n_n f_N}} \tag{10}$$

### 4.1.3 Simplified Model of Lattice Stud

The CFSTT shear walls adopt double- or four-limb latticed studs, which composed of two or four square steel tubes connected by galvanized V-shaped connectors respectively. This structure is much more complex than cold-formed thin-walled C steel. Therefore, in order to establish FE analysis model, this paper proposed a simplified model to systematically reduce the number of assembled wall members.

In order to simplify the analysis, galvanized V-shaped connectors were idealized as tilted belly poles of concrete filled steel tubular (CFST) column. Specifically, the bending stiffness of the steel tube concrete frame structure  $B_f$  was expressed as Eq. (11) (Nie et al. 2008):

$$B_f = \gamma(E_s I_s + \alpha \cdot E_c I_c) \tag{11}$$

where,  $E_s I_s$  and  $E_c I_c$  represent elastic stiffness of steel and concrete respectively;  $\alpha$  is the stiffness reduction coefficient of concrete infill, which is related with the cross-section of the steel tube; for the circular steel tube,  $\alpha = 0.8$ , and for the square steel tube,  $\alpha = 0.6$ ;  $\gamma$  is column stiffness reduction factor.

In this paper,  $E_c I_c = 0$ , so  $B_f = \gamma E_s I_s$ . For single limb stud,  $\gamma = 1.0$ ; for latticed stud,  $\gamma$  is obtained according to Eq. (12).

$$\gamma = \frac{1}{1 + m \frac{E_{sc} A_{sc}}{E_w A_w}} \tag{12}$$

in which,  $E_{sc} A_{sc}$  is section stiffness of a column in compression;  $E_w A_w$  represents section stiffness of tilted belly pole; as for double-limb latticed studs or four-limb latticed studs,  $m$  and  $C_1$  was given by:

$$m = 4.23 \frac{C_1}{n^2} \tag{13}$$

$$C_1 = \frac{1}{1 + k_1^3 (1/k_2 - 1)} \tag{14}$$

$$k_1 = \frac{H_t}{H} \tag{15}$$

$$k_2 = \frac{I_t}{I_d} \tag{16}$$

where,  $n$  is internode number;  $H_t$  is height of upper column;  $H$  is height of whole column;  $I_t$  and  $I_d$  are section inertia of upper and bottom columns, respectively.

According to the theory of CFST column, the wall studs of shear walls were simplified as seen in Fig. 13. In this paper, latticed stud was simplified as constant section stud, so  $k_1 = k_2 = 1.0$  and  $C_1 = 1.0$ . Besides,  $n = 4$ ,  $E_w A_w = 12,407.35 \text{ kN}$  and  $E_{sc} A_{sc} = 93,324 \text{ kN}$  can be obtained. On the base of the above mentioned formulas, the stiffness reduced factor of the column  $\gamma = 0.906$  can be calculated. According to the description in Sect. 2.3, the wall studs were assumed without moment along the out of plane direction during the loading process.

In attempt to simplify double- or four-limb latticed stud into a square steel tube, the thickness of the steel tube was assumed to be unchanged. Two assumed methods were presented to consider the dimensions along or perpendicular to the wall: (1)  $b_1 = b_2$ , as shown in Fig. 14a; (2)  $h_1 = h_2$ , as shown in Fig. 14b. According to the analysis above, the dimensions of the simplified cross section in another direction can be determined. The prerequisite of determining the dimensions was that the rotational stiffness of the in-plane simplified section (i.e., the rotational stiffness around the Y axis) is equal to that of the origin section and the influence of the column stiffness reduction  $\gamma$  should also be taken into consideration. The simplified calculation was expressed as follows: as for the original section, rotational inertia of the

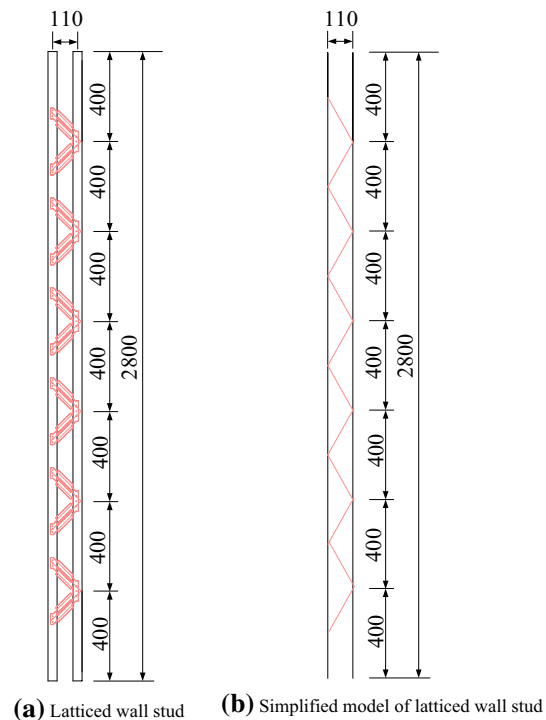


Fig. 13 Simplified model of latticed wall stud

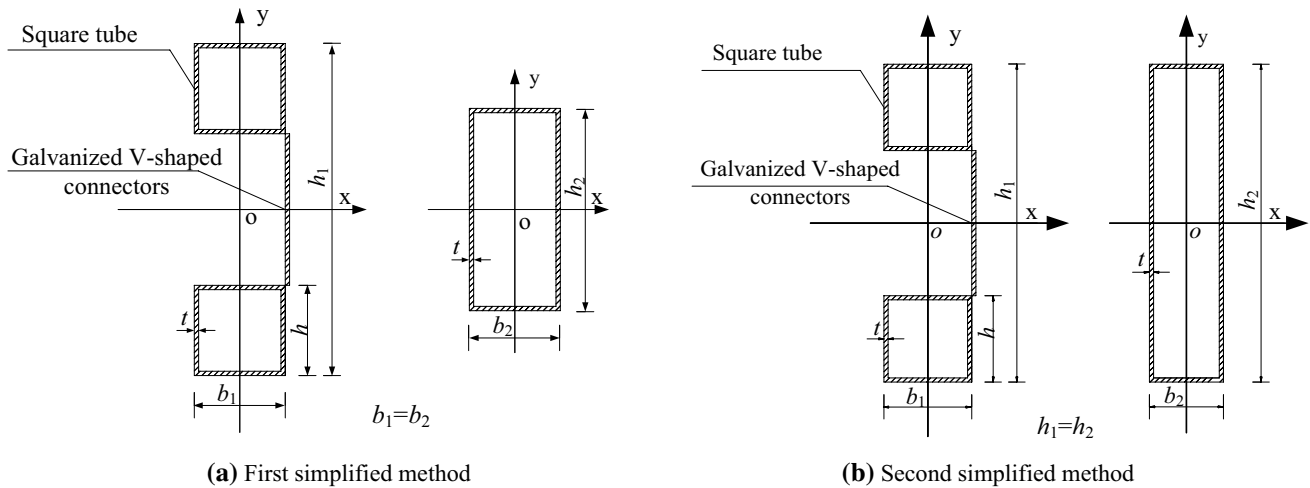


Fig. 14 Simplified calculation methods of double-limb latticed stud section

Y-axis  $E_s I_{sy1}$  is  $2.31 \times 10^{10} \text{ Nmm}^2$  ( $E_s = 2.02 \times 10^5 \text{ N/mm}^2$ ,  $I_{sy1} = 114,306.5 \text{ mm}^4$ ). Besides, as for the simplified section, bending stiffness about Y-axis is  $B_f = \gamma E_s I_{sy1} = 0.906 \times 2.31 \times 10^{10} = 2.09 \times 10^{10} \text{ Nmm}^2$ .

Since it was assumed that  $b_1 = b_2 = 40 \text{ mm}$  on the base of the first hypothesis, the value of  $h_2$  can be obtained by substituting  $b_2$  and  $b_1$  into Eq. (15):

$$B_f = \gamma E_s I_{sy1} = E_s I_{sy2} = 2.02 \times 10^5 \left[ \frac{1}{12} h_2 \times 40^3 - \frac{1}{12} (h_2 - 3)(40 - 3)^3 \right] \quad (17)$$

thus,  $h_2 = 81.638 \text{ mm}$  can be obtained.

Similarly,  $b_2$  can be obtained by substituting the value of  $h_1$  and  $h_2$  ( $h_1 = h_2 = 150 \text{ mm}$ ) into Eq. (16) and considering the second hypothesis:

$$B_f = \gamma E_s I_{sy1} = E_s I_{sy2} = 2.02 \times 10^5 \left[ \frac{1}{12} \times 150 \times b_2^3 - \frac{1}{12} \times 147 \times (b_2 - 3)^3 \right] \quad (18)$$

$b_2 = 81.638 \text{ mm}$  can be obtained.

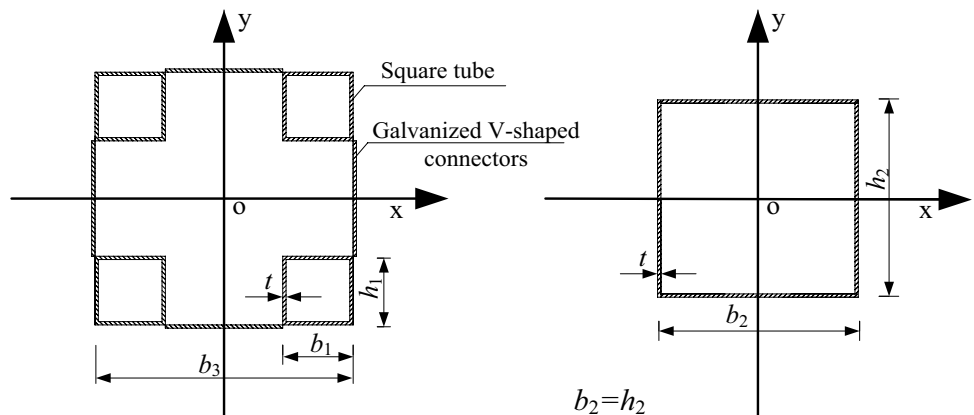
When the four-limb latticed column was simplified to square steel tube column, it was assumed that the rectangular steel tube had the same size ( $b_2 = h_2$ ) along the two directions considering the effect of symmetry; besides, the thickness of the steel tube  $t$  was fixed (seen in Fig. 15). In the analysis above, original section rotational inertia around the Y-axis can be calculated,  $E_s I_{sy1} = 6.11 \times 10^{11} \text{ Nmm}^2$  ( $E_s = 2.02 \times 10^5 \text{ N/mm}^2$ ,  $I_{sy1} = 3,023,713 \text{ mm}^4$ ). The bending stiffness about Y-axis  $B_f = E_s I_{sy1} = 0.906 \times 6.11 \times 10^{10} = 5.54 \times 10^{10} \text{ Nmm}^2$ . Hence,  $b_2 = h_2 = 141.470 \text{ mm}$ .

## 4.2 Restoring Force Model of CFSTT Shear Walls

### 4.2.1 Degraded Four-Line Model

A degraded four-line model (Ye et al. 2016) was adopted to suit the load–displacement envelope curves for all specimens, owing to the notable distinction between the two

Fig. 15 Simplified calculation method of four-limb latticed stud section



components with different material properties connected by screws. The envelope curve was simulated by degraded four-line model in accordance with the variation rule of load displacement curves about CFSTT shear walls, as displayed in Fig. 17. Degraded four-line model can represent pinched load deformation response with the ability to appear degradation under cyclic loading. The entire envelope of hysteretic behavior could be obtained based on this 4-point envelope curve.

Elastic stage (0–1): point 1 was defined as elastic limit of CFSTT shear wall (i.e.  $0.4F_p$ ,  $F_p$  is the shear bearing capacity of the wall).

Yield stage (1–2): point 2 was defined as yield point; the point corresponding to the load and displacement are named yield load  $F_y$  and yield displacement  $\Delta_y$ , respectively.

Hardening stage (2–3): define point 3 as peak point. The point corresponding to the load and displacement are named peak load  $F_p$  and peak displacement  $\Delta_p$ , respectively.

Strength degradation stage (3–4): define point 4 as failure point. The point corresponding to the load and displacement are named failure load  $F_f$  and failure displacement  $\Delta_f$ , respectively.

$K_1$ ,  $K_2 = \gamma_1 K_1$ ,  $K_3 = \gamma_2 K_1$ , and  $K_4 = \gamma_3 K_1$  are the corresponding stiffness in the four different stages, which are respectively defined as the slopes of the lines linking adjacent points. In which,  $\gamma_1, \gamma_2, \gamma_3$  are experimental regression coefficients. The stiffness can be obtained from Fig. 16. As the result of experiment, Degraded four-line model of specimen was presented in Fig. 17. The stiffness of each stage corresponding to each specimen was listed in Tables 6 and 7 listed the results of  $\gamma_1, \gamma_2, \gamma_3$  which conform to the order  $\gamma_1 > \gamma_2 > \gamma_3$ , confirming the stiffness degradation. This

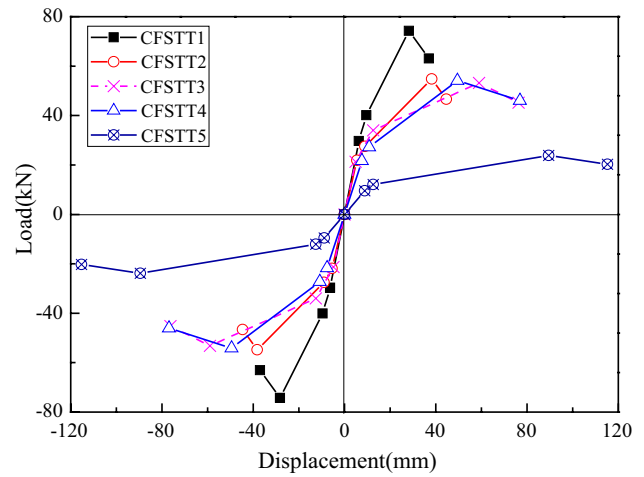


Fig. 17 Degraded four-line models of wall specimens

envelope curve provides a simplified method to analysis CFSTT shear walls.

#### 4.2.2 Unloading Stiffness Degradation

As the load–displacement envelope curve illustrated in Fig. 18, the unloading stiffness decreased with the increase of displacement amplitude. The unloading stiffness of each specimen can be obtained by formula (17). Table 8 listed the values of unloading stiffness regression coefficient of each specimen corresponding to yield point, ultimate point and failure point. In the case of unloading between the feature points, the regression coefficients of the unloading stiffness can be obtained by displacement interpolation (Huang et al. 2016).

Fig. 16 Degraded four-line model

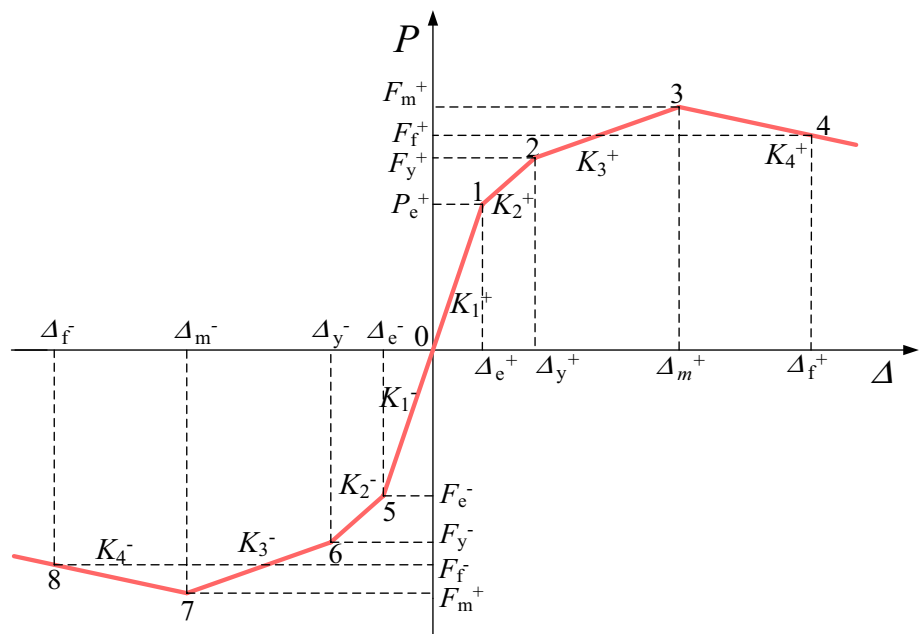


**Table 6** Stiffness of shear wall specimens in each stage

Specimen number	Stiffness in each stage (kN/mm)			
	$K_1$	$K_2$	$K_3$	$K_4$
CFSTT1	4.681	3.263	1.827	-1.259
CFSTT2	3.998	1.601	0.934	-1.282
CFSTT3	4.409	1.641	0.414	-0.460
CFSTT4	2.840	1.743	0.696	-0.296
CFSTT5	1.086	0.661	0.154	-0.135

**Table 7** Experimental regression coefficients of shear wall specimens

Specimen number	$\gamma_1$	$\gamma_2$	$\gamma_3$
CFSTT1	0.697	0.390	-0.269
CFSTT2	0.400	0.234	-0.321
CFSTT3	0.693	0.094	-0.104
CFSTT4	0.614	0.245	-0.104
CFSTT5	0.609	0.142	-0.124

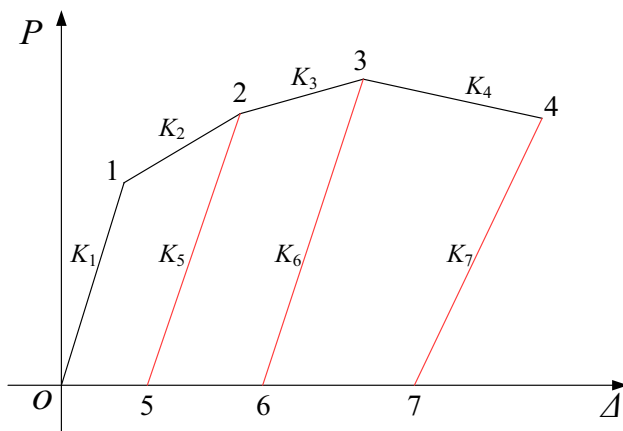


**Fig. 18** Unloading stiffness degradation

**Table 8** Unloading stiffness regression coefficients of shear wall specimens

Specimen number	$\lambda_1$	$\lambda_2$	$\lambda_3$
CFSTT1	0.275	-0.083	-0.400
CFSTT2	-0.053	-0.248	-0.574
CFSTT3	-1.372	-0.835	-0.848
CFSTT4	-0.064	-0.550	-0.755
CFSTT5	-0.395	-0.625	-

In stage (1 – 2) :  $\frac{K}{K_1} = \left(\frac{\Delta}{\Delta_e}\right)^{\lambda_1}$  ,  $\Delta_e < |\Delta| < \Delta_y$  (17a)

In stage (2 – 3) :  $\frac{K}{K_1} = \left(\frac{\Delta}{\Delta_e}\right)^{\lambda_2}$  ,  $\Delta_y < |\Delta| < \Delta_p$  (17b)

In stage (3 – 4) :  $\frac{K}{K_1} = \left(\frac{\Delta}{\Delta_e}\right)^{\lambda_3}$  ,  $\Delta_p < |\Delta| < \Delta_f$  (17c)

where,  $K$  represents unloading stiffness of shear walls;  $\Delta$  is displacement of shear wall during unloading;  $\lambda_1, \lambda_2, \lambda_3$  are unloading stiffness coefficients;  $K_1$  is elastic stiffness of envelope curve of the shear walls.

### 4.2.3 Pivot Model

As a matter of fact, the software SAP2000 provides various hysteretic material models (including Kinematic, Takeda, and Pivot), while particularly, pivot model owns the better ability to predict the pinched hysteretic behavior to sheathing-to-frame connections in CFS shear walls. The method of using Pivot hysteretic model was first put forward by Dowell et al. (1998) on the basis of the observation that the hysteresis curve of specimens was inclined to some special points (pivot points) of two direction of loading and unloading.

As illustrated in Fig. 19, the quadrants  $Q_1, Q_2, Q_3$  and  $Q_4$  are delimited by the initial elastic branches defined before (not the vertical force axis) and the abscissa axis. A sample point (in the force–displacement plane) is placed in each quadrant. The arrows extending from the points (point 1, 2, 3 and 4) represent potential loading or unloading paths in the force–displacement plane. The pivot model is composed of six characteristic points including  $PP_1, PP_2, P_1, P_2, P_3, P_4$ , which are controlled by four parameters ( $\alpha_1, \alpha_2, \beta_1$  and  $\beta_2$ ) and the load which corresponded to the first turning point on the load–displacement envelope curve. The relative values of  $\alpha_1, \alpha_2, \beta_1$  and  $\beta_2$  are referred to the control points corresponding to situation: unloading the positive force to zero, unloading the negative force to zero, loading from zero to positive and loading from zero to negative, respectively.

## 5 Test Verification

With regard to the test data, the simplified numerical analysis method for researching the seismic response of CFSTT shear wall is an effective measure to cut down money and time expending on further investigations. OSB sheathing-to-frame connections were stimulated using the nonlinear link element with a multi-linear backbone curve, which represented the main nonlinear source in the walls. The simplified model of the CFSTT shear wall was shown in Fig. 20. Experiments on five CFSTT shear walls were conducted to confirm the rationality of the



**Fig. 19** Multi-linear plastic pivot hysteresis model principle

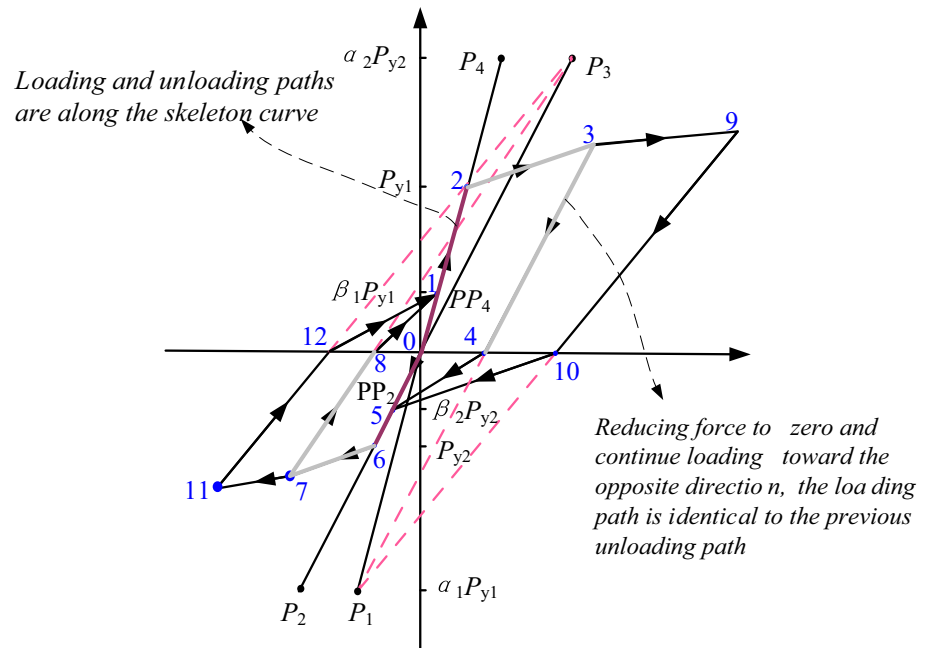
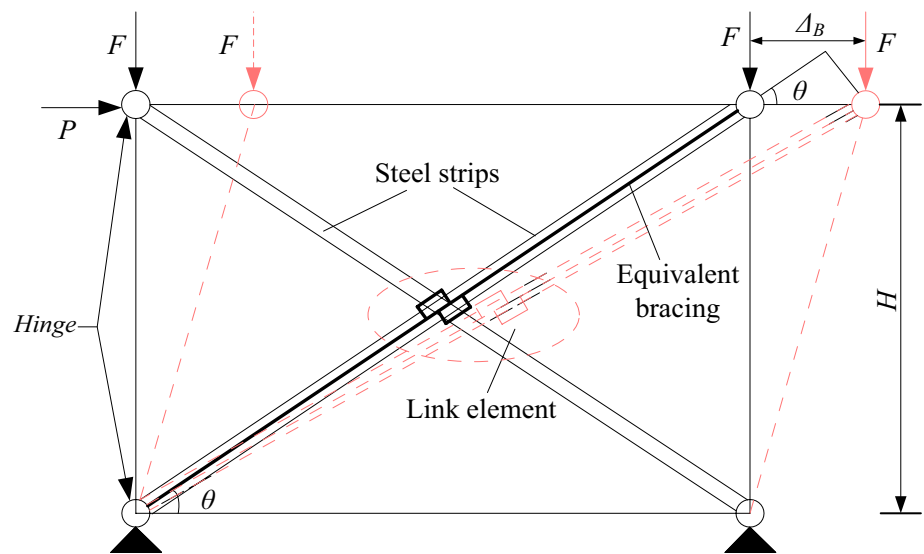


**Fig. 20** Simplified model of CFSTT shear wall



proposed method. The test results were compared to various types of shear wall models based on FE analysis using software SAP2000, which taking the shear wall envelope curve and Pivot parameters (see Fig. 21) into account. It is assumed that the shear walls have symmetric loading path of forward and reverse loading because that the loading of two directions have similar eigenvalue. Thus,  $\alpha_1 = \alpha_2$ ,  $\beta_1 = \beta_2$ . The various values of the coefficients  $\alpha_1$ ,  $\alpha_2$ ,  $\beta_1$  and  $\beta_2$  of each specimen are as shown in follows: for CFSTT1,  $\alpha_1 = \alpha_2 = 12$  and  $\beta_1 = \beta_2 = 0.08$ ; for CFSTT2-4,  $\alpha_1 = \alpha_2 = 19$  and  $\beta_1 = \beta_2 = 0.1$ ; for CFSTT5,  $\alpha_1 = \alpha_2 = 6$  and  $\beta_1 = \beta_2 = 0.15$ .

Test results obtained from CFSTT specimens were employed to assess the accuracy and validity of the simplified numerical analysis model. The predicted and experimental hysteretic curves and envelope curves had been respectively compared in Figs. 5 and 6. With respect to the later load versus displacement hysteretic curves, analytical and experimental results were in good agreement. Besides, the numerical results appeared similar hysteretic curves, pinching effect and unloading paths with the test results. Moreover, the analytical and experimental results were coincided in linear relationship. Table 9 summarized the predicted and test data of the five shear wall specimens.

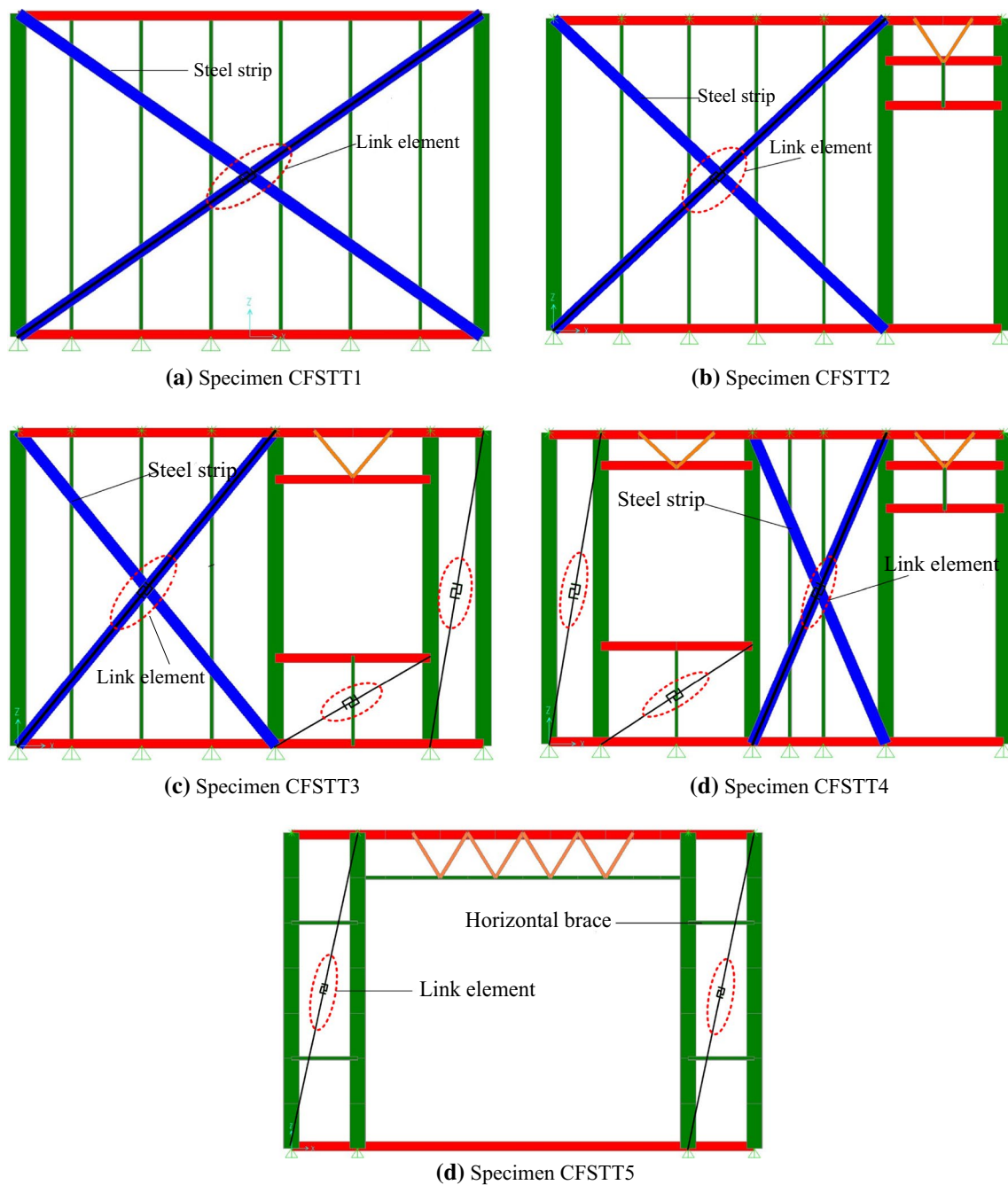


**Fig. 21** Modeling of CFSTT shear walls in software SAP2000

Moreover, the predicted results of the three typical characteristic points and elastic stiffness were agreed well with the test data. It was also noted that the elastic stiffness of the FE models in third quadrant were relatively larger than that of the tested results for the differences in the imperfection, actual loading condition and material damage. Consequently,

it was demonstrated that the proposed simplified model was reasonable for CFSTT shear walls, and the nonlinear simplified analysis method can be applied in seismic analysis of CFSTT shear walls. In addition, the method was also available for the study of the elastic–plastic seismic performance analysis of CFSTT global structures.

**Table 9** Comparison of shear wall specimens between tested and predicted results

Specimen number	Test results					Predicted results				
	$P_{y,t}$ (kN)	$\Delta_{y,t}$ (mm)	$P_{p,t}$ (kN)	$\Delta_{p,t}$ (mm)	$K_{e,t}$ (kN/mm)	$P_{y,c}$ (kN)	$\Delta_{y,c}$ (mm)	$P_{p,c}$ (kN)	$\Delta_{m,c}$ (mm)	$K_{e,c}$ (kN/mm)
CFSTT1	40.12	10	74.22	28	7.78	46.49	12	72.47	37	6.06
CFSTT2	27.48	9	54.80	38	6.12	26.31	11	50.75	40	4.77
CFSTT3	34.01	13	53.21	59	4.23	32.98	11	54.31	39	4.82
CFSTT4	27.25	11	54.12	50	5.00	29.60	12	58.58	50	4.76
CFSTT5	12.08	13	23.89	89	1.90	15.83	14	26.69	61	1.87

$P_{y,t}$  and  $P_{m,t}$  are respectively yield load and peak load of experiment results;  $\Delta_{y,t}$  and  $\Delta_{m,t}$  are respectively yield displacement and peak displacement of experiment tests;  $K_{e,t}$  is the test value of elastic stiffness;  $P_{y,c}$  and  $P_{m,c}$  are respectively yield load and peak load of predicted results;  $\Delta_{y,c}$  and  $\Delta_{m,c}$  are respectively yield displacement and peak displacement of predicted results;  $K_{e,c}$  is the predict value of elastic stiffness

## 6 Conclusion

In this paper, five full-scale shear walls subjected to low cyclic loading and a nonlinear simplified FE modeling was established and verified by the experimental results. Base on the experimental and analytical data in this paper, the conclusions may be concluded as follows:

- (1) The diaphragm effect had a favorable influence on hysteretic behavior and energy-dissipating capacity of the CFSTT shear walls. Nevertheless, the different type of wall openings would weaken seismic behavior of the CFSTT shear walls. Setting four-limb lattice studs for the CFSTT shear wall is a reliable method to enhance its shear resistance.
- (2) The seismic response of the shear wall can be predicted by equivalent tie rod with nonlinear elements. The simplified model of double- or four-limb latticed studs and OSB panels was developed and it can be concluded that it is suitable enough to be used to carry out a study for stimulating the seismic behavior of shear walls.
- (3) The restoring force properties can be defined using degraded four-line model on the base of the later load versus displacement hysteretic curve of the shear wall. Pivot hysteretic model with multiple linear elastic link units was used in the FE model, and a series of nonlinear analysis conditions are defined to predict the seismic performance of CFSTT shear wall.
- (4) The nonlinear simplified analysis modeling on CFSTT shear wall was established and verified by the experimental data in term of failure pattern and load–displacement relation curves in this study. Thus, it proved that the nonlinear simplified analysis models could be used to predict the seismic performance of this type of CFSTT shear wall with an acceptance precision.

**Acknowledgements** This work described in paper is supported by the National Natural Science Foundation of China (Project 51478158) and the New Century Excellent Talents in University (Project NCET-12-0838); the authors greatly appreciated the support.

## References

- AISI-S213-07/S1-09. (2007). *North American standard for cold-formed steel framing-lateral design*. Edition with supplement no. 1, American Iron and Steel Institute.
- ATC-24. (1992). *Guidelines for cyclic seismic testing of components of steel structures*. Redwood City, CA: Applied Technology Council.
- Buonopane, S. G., Bian, G., Tun, T. H., et al. (2015). Computationally efficient fastener-based models of cold-formed steel shear walls with wood sheathing. *Journal of Constructional Steel Research*, 110, 137–148.

- CAN/CSA S136-01. (R2007). *North American specification for the design of cold formed steel structural members*. Canadian Standards Association.
- Casafont, M., Arnedo, A., Roure, F., et al. (2006). Experimental testing of joints for seismic design of lightweight structures. Part 1. Screwed joints in straps. *Thin-Walled Structures*, 44(2), 197–210.
- DB34/T1262-2010. (2010). *Technical specification for concrete-filled steel tubular structures*. Anhui. (in Chinese).
- Design Manual for light gauge steel structures. (2002). Gihodo Shuppan Co., Ltd. (in Japanese).
- Dowell, R. K., Seible, F., & Wilson, E. L. (1998). Pivot hysteresis model for reinforced concrete members. *ACI Structural Journal*, 95(5), 607–617.
- Fiorino, L., Shakeel, S., Macillo, V., et al. (2018). Seismic response of CFS shear walls sheathed with nailed gypsum panels: Numerical modeling. *Thin-Walled Structures*, 122, 359–370.
- Fiorino, L., Terracciano, M. T., & Landolfo, R. (2016). Experimental investigation of seismic behaviour of low dissipative CFS strap-braced stud walls. *Journal of Constructional Steel Research*, 127, 92–107.
- Fülöp, L. A., & Dubina, D. (2004). Performance of wall-stud cold-formed shear panels under monotonic and cyclic loading part II: Numerical modeling and performance analysis. *Thin-Walled Structures*, 42, 339–349.
- GB/T 17657-2013. (2013) *Test methods of evaluating the properties of wood-based panels and surface decorated wood-based panels*. Standards Press of China. (in Chinese).
- GB/T228-2010. (2010). *Metallic materials-tensile testing at ambient temperature*. Beijing: Architecture Industrial Press of China. (in Chinese).
- Huang, Z. G., Wang, Y. J., Su, M. Z., et al. (2016). Study on restoring force model of cold-formed steel wall panels and simplified seismic response analysis method of residential buildings. *China Civil Engineering Journal*, 45(2), 26–34. (in Chinese).
- JGJ/T 101-2015. (2015). *Specification for seismic test of buildings*. Beijing: Architecture Industrial Press of China. (in Chinese).
- JGJ101-96. (1997). *Specification for test methods of seismic buildings*. Beijing: Architecture Industrial Press of China. (in Chinese).
- Kim, T., Wilcoski, J., Foutch, D. A., et al. (2006). Shakedown tests of a cold-formed steel shear panel. *Engineering Structures*, 28(10), 1462–1470.
- Langea, J., & Naujoksb, B. (2006). Behaviour of cold-formed steel shear walls under horizontal and vertical loads. *Thin-Walled Structures*, 44(12), 1214–1222.
- Lee, Y. K., & Miller, T. H. (2001). Axial strength determination for gypsum-sheathed, cold-formed steel wall stud composite panels. *Journal of Structural Engineering*, 127(6), 608–615.
- Li, Y. L., Li, Y. Q., & Shen, Z. Y. (2016). Investigation on flexural strength of cold-formed thin-walled steel beams with built-up box section. *Thin-Walled Structures*, 107, 66–79.
- Li, Y. Q., Li, Y. L., Wang, S. K., & Shen, Z. Y. (2014). Ultimate load-carrying capacity of cold-formed thin-walled columns with built-up box and I section under axial compression. *Thin-Walled Structures*, 79, 202–217.
- LY/T 1580-2010. (2010). *Oriented strand board*. Beijing: Standards Press of China. (in Chinese).
- Magnucka-Blandzi, E., & Magnucki, K. (2011). Buckling and optimal design of cold-formed thin-walled beams: Review of selected problems. *Thin-Walled Structures*, 49(5), 554–561.
- Meddah, H., Berediaf-Bourahla, M., El-Djouzi, B., et al. (2016). Numerical analysis of cold-formed steel shear wall panels subjected to cyclic loading. *International Journal of Civil, Environmental, Structural, Construction and Architectural Engineering*, 12(10), 1456–1461.
- Mohebbi, S., Mirghaderi, R., Farahbod, F., & Sabbagh, A. B. (2015). Experimental work on single and double-sided steel sheathed cold-formed steel shear walls for seismic actions. *Thin-Walled Structures*, 91, 50–62.
- Niari, S. E., Rafezy, B., & Abedi, K. (2015). Seismic behavior of steel sheathed cold-formed steel shear wall: Experimental investigation and numerical modeling. *Thin-Walled Structures*, 96, 337–347.
- Nie, S. F., Zhou, T. H., Zhou, X. H., et al. (2008). Research on lateral stiffness of cold-formed steel composite wall. *Journal of Chongqing Jianzhu University*, 2, 75–79. (in Chinese).
- Nithyadharan, M., & Kalyanaraman, V. (2012). Behavior of cold-formed steel shear wall panels under monotonic and reversed cyclic loading. *Thin-Walled Structures*, 60(11), 12–23.
- Obst, M., Kurpisz, D., & Paczos, P. (2016). The experimental and analytical investigations of torsion phenomenon of thin-walled cold formed channel beams subjected to four-point bending. *Thin-Walled Structures*, 106, 179–186.
- Ostwald, M., & Rodak, M. (2013). Multicriteria optimization of cold-formed thin-walled beams with generalized open shape under different loads. *Thin-Walled Structures*, 65, 26–33.
- Peterman, K. D., Nakata, N., & Schafer, B. W. (2014). Hysteretic characterization of cold-formed steel stud-to-sheathing connections. *Journal of Constructional Steel Research*, 101, 254–264.
- Schafer, B. W., Ayhan, D., Leng, J., Liu, P., et al. (2016). Seismic response and engineering of cold-formed steel framed buildings. *Structures*, 8, 197–212.
- Shahbazian, A., & Wang, Y. C. (2012). Direct strength method for calculating distortional buckling capacity of cold-formed thin-walled steel columns with uniform and non-uniform elevated temperatures. *Thin-Walled Structures*, 53, 188–199.
- Tian, Y. S., Wang, J., & Liu, T. J. (2007). Axial load capacity of cold-formed steel wall stud with sheathing. *Thin-Walled Structures*, 45(5), 537–551.
- Wang, J. F., Wang, F. Q., Shen, Q. H., et al. (2019). Seismic response evaluation and design of CTSTT shear walls with openings. *Journal of Constructional Steel Research*, 153, 550–566.
- Wang, X. X., & Ye, J. H. (2016). Cyclic testing of two- and three-story CFS shear-walls with reinforced end studs. *Journal of Constructional Steel Research*, 121, 13–28.
- Xu, Z. F., Chen, Z. F., Osman, B. H., & Yang, S. (2018). Seismic performance of high-strength lightweight foamed concrete-filled cold-formed steel shear walls. *Journal of Constructional Steel Research*, 143, 148–161.
- Ye, J. H., Wang, X. X., Jia, H. Y., & Zhao, M. Y. (2015). Cyclic performance of cold-formed steel shear walls sheathed with double-layer wallboards on both sides. *Thin-Walled Structures*, 92, 146–159.
- Ye, J. H., Wang, X. X., & Zhao, M. Y. (2016). Experimental study on shear behavior of screw connections in CFS sheathing. *Journal of Constructional Steel Research*, 121, 1–12.
- Zeynalian, M., & Ronagh, H. R. (2012). A numerical study on seismic performance of strap-braced cold-formed steel shear walls. *Thin-Walled Structures*, 60, 229–238.

**Publisher's Note** Springer Nature remains neutral with regard to jurisdictional claims in published maps and institutional affiliations.